Multi-antenna GNSS and INS/Odometer Coupling for Robust Vehicular Navigation

Niranjana Vagle, Ali Broumandan and Gérard Lachapelle
Department of Geomatics Engineering
Schulich School of Engineering
University of Calgary
Email : vaglen@ucalgary.ca, abrouman@ucalgary.ca, lachapel@ucalgary.ca

BIOGRAPHIES

Niranjana Vagle received his PhD degree in Geomatics Engineering from the University of Calgary. His main research interests are antenna array signal processing techniques and sensor integration for GNSS applications.

Ali Broumandan received his Ph.D. degree in the Geomatics Engineering from the University of Calgary. He is working in the PLAN Group as Senior Research Associate since November 2013 and his research focuses on GNSS interference mitigation utilizing single and multiple antenna processing. He has been involved in several industrial research projects focusing on spatial/temporal GNSS signal processing.

Gérard Lachapelle, Professor Emeritus, has been involved in a multitude of GNSS R&D projects since 1980, ranging from RTK positioning to indoor location and signal processing enhancements, first in industry and since 1988, at the University of Calgary.

ABSTRACT

With increasing focus on using Global Navigation Satellite Systems (GNSS) in autonomous navigation and related technologies, it is important to provide robust navigation solutions. Radio frequency interference, either intentional or unintentional, has a direct impact on navigation performance. In terms of security, spoofing is the major issue that users are concerned about. This paper focuses on multi-antenna GNSS and Inertial Navigation System (INS)-odometer integration to provide robust navigation solutions. Multi-antenna GNSS provides robustness against different interference sources and integration with INS provides continuous navigation solutions during short-term signal outages. Performance of the proposed architecture is evaluated using different user scenarios in the presence of spoofing and interference signals.

1 INTRODUCTION

GNSS provides seamless solutions in open sky environments with good satellite visibility. However, its performance is limited in degraded environments such as urban canyons, foliage conditions (tree canopy) and fails to provide continuous solutions. Apart from the satellite visibility concern, GNSS signals intrinsically have low power, which makes them open to different interference scenarios including deliberate spoofing and jamming. Spoofing is a wideband interference which misguides users with incorrect solutions. This paper focusses on defining a system architecture using an array of antennas to counteract against different interference attacks and provides robust solutions for vehicular applications.

GNSS and INS have complementary error characteristics: GNSS has good long term accuracy, whereas INS has good short term accuracy. INS is self-contained, operates continuously and provides navigation solutions with low short term noise. However, it suffers from accuracy degradation over time due to the integration of biases and drifts of the Inertial Measurement Units (IMUs) over time. Along with navigation solutions, attitude information can also be estimated from INS, which is of importance in beamforming applications. The complementary features of GNSS and INS make them a good choice for integration especially when GNSS observability is poor. Advantages and performance of loosely, tightly and ultra-tightly coupled GNSS/INS integration methods have been studied and reported by a number of researchers [1-4]. In a typical GNSS-INS system, an IMU with three accelerometers and three gyroscopes is used. For land based vehicular applications, a reduced number of sensors known as a Reduced Inertial Sensor System (RISS) [5] can be used to reduce cost. Even though, integration of GNSS and RISS provides robust navigation, performance will be degraded under spoofing or any other jamming attacks. Under these scenarios, GNSS measurements will be erroneous which in turn makes the integrated solution unreliable.

Different interference mitigation techniques have been studied in the literature. Most of these techniques are based on different signal processing methods using single antenna. However, antenna array based techniques are known to be the most effective against all types of interference including jamming and spoofing signals. For spoofing attacks, most of the research has focused on detecting spoofing attacks and alerting the receiver of such attacks. However, to provide continuous navigation solutions along with spoofing detection, it is also necessary to mitigate it. Performance of different spoofing detection and mitigation techniques have been studied under different spoofing scenarios [6-13]. Some of these techniques include monitoring the incoming signal power by measuring Carrier-to-Noise (C/N_0) density ratio [8],

AGC monitoring [9], checking the power content of the GNSS signals at the pre-despreading level [10], and network based signal authentication [6]. Most of the commercial receivers available in the market today are using more than one constellation. These multi-constellation receivers provide further robustness against spoofing attacks as it would be complex and expensive to simultaneously spoof different constellations [14]. Antenna array based GNSS receivers have been studied extensively to mitigate different interference scenarios including spoofing [15-16]. Spatial discrimination based approaches using antenna arrays are effective methods to deal with most spoofing attacks. An antenna array based GNSS receiver consists of several antennas placed at a distance of half of the carrier wavelength. Usually, spoofing signals will be received from a different direction than that of authentic signals which can be exploited in the antenna array processing techniques to place a null in the direction of the spoofer.

In an antenna array based GNSS receiver, signals from different antenna elements can be combined using different beamforming/null-steering techniques. However, some of these techniques induce distortions in the measurements in the presence of interference. It has been shown that the Minimum Power Distortionless Response (MPDR) beamformer induces minimal distortions in both code and carrier phase measurements [20]. MPDR beamformer points the main beam in the direction of a desired satellite while reducing power of other unwanted interference. To point the beam in the direction of the desired satellite, both platform attitude and direction of the satellite are necessary. By using almanac or ephemeris information, direction of the satellite can be obtained. The receiver attitude can be obtained from the INS which is mounted on the same platform. Thus, to provide protection against different types of interference and yet provide distortionless measurements and robust navigation, it is necessary to integrate antenna array based GNSS receivers with INS.

To this end, an integration of antenna array based GNSS receiver with RISS is investigated in this work. The RISS in this case consists of one single-axis gyroscope and a two-axis accelerometer along with vehicle odometer to obtain 3D navigation solutions. A four-element antenna array is considered. GNSS and INS are loosely coupled. To perform MPDR beamforming, vehicle heading information is obtained from the RISS. Integrated multi-antenna GNSS-RISS provides several advantages including (a) robust anti-spoofing approach as consistency check can be performed using both antenna array and IMU, (b) RISS provides heading information for antenna array receiver to perform distortionless beamforming and robust and continuous navigation solutions. Advantages of such integrated system are studied using different scenarios.

In Section 2, the system architecture used for multi-antenna GNSS and INS loose coupling is discussed. Section 2 also discusses implementation details, different spoofing simulation scenarios and beamforming methods. Data collection scenarios and discussion of the results are presented in Section 3 and 4 respectively.

2 METHODOLOGY

This section describes the overall architecture of the GNSS-RISS integration filters and beamforming techniques. In addition, the spoofing signal simulations are described.

2.1 System Architecture

The overall system architecture of the integrated multi-antenna GNSS receiver and RISS used herein is shown in Figure 1. The multi-antenna receiver consists of a rectangular 4-element antenna array connected to a synchronized 4-channel front-end. Signals from different antenna elements are acquired, tracked and combined using MPDR beamforming in the post-correlation stage. The combined correlation values are used to drive code and carrier tracking loops. The replica signals generated from these loops are used to despread incoming signals from different antenna elements. The combined correlation values are also used to generate pseudorange and delta range measurements. The roll and pitch information is obtained using two accelerometers and the heading from the vertical gyroscope. This attitude information along with the satellite direction of arrival information is used in the MPDR beamforming to mitigate interference and direct the beam in the direction of satellite. The covariance matrix for the beamformer is computed at the pre-despreading process. For the spoofing scenarios, since all the spoofed signals are assumed to be arriving from the same direction, the spatial power will be higher than that of authentic signals. Hence, by constructing the covariance matrix in the pre-despreading stage, the beamformer can suppress interference including spoofing. The measurements from the multi-antenna receiver and the mechanized solution from RISS are fed to the navigation filter which consists of position estimation filters to compute position from GNSS only and GNSS-RISS combined. Figure 1 shows navigation filters for loose coupling. A Kalman Filter (KF) estimator is used to compute position and velocity from GNSS measurements to be used in loose coupling. In this case, GNSS position and velocity are combined with RISS solutions using KF.

2.2 Beamforming Approach

MPDR beamformer points the beam in the direction of the desired satellite while reducing the power of other unwanted interference sources. The optimum weight vector for the MPDR beamformer for the j^{th} satellite is given by [24]

$$\mathbf{w}_j^{\mathrm{MPDR}} = \frac{\mathbf{R}_{\mathbf{xx}}^{-1}\mathbf{a}_j}{\boldsymbol{a}_j^H \mathbf{R}_{\mathbf{xx}}^{-1}\mathbf{a}_j} \quad (1)$$

The covariance matrix R_{xx} is computed at the pre-despreading stage and a_j is the steering vector of the j^{th} satellite in the body frame.

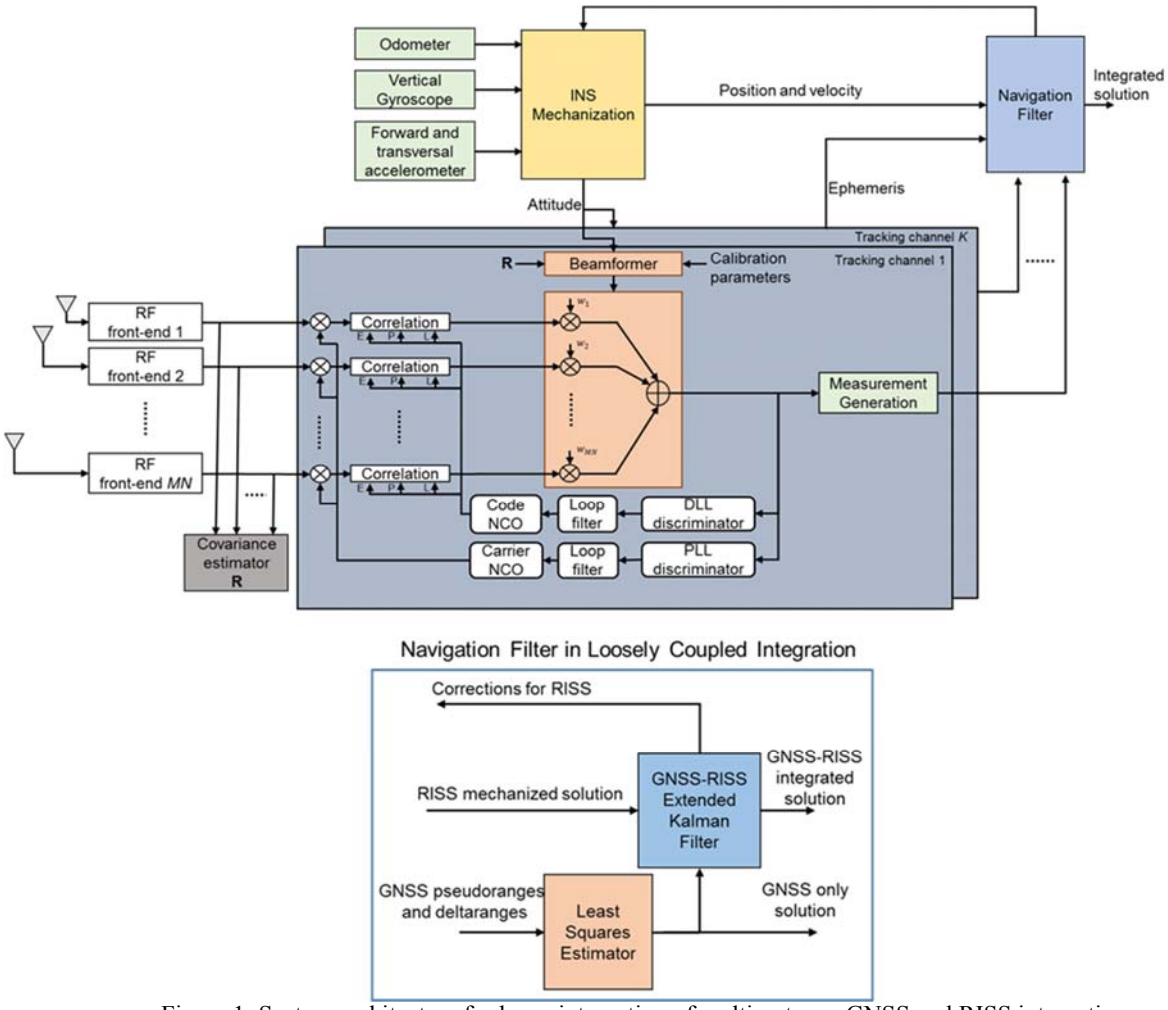

Figure 1: System architecture for loose integration of multi-antenna GNSS and RISS integration

To compute the steering vector, the array configuration and Angle-of-Arrival (AOA) of the satellite in the body frame is required. The steering vector for a MxN rectangular array is given by

$$\mathbf{a}_j = \begin{bmatrix} 1 \\ e^{i\frac{2\pi}{\lambda_{GNSS}}\left(\xi_j^B\right)^T p_{1,2}} \\ . \\ . \\ e^{i\frac{2\pi}{\lambda_{GNSS}}\left(\xi_j^B\right)^T p_{M,N}} \end{bmatrix} \quad (2)$$

where ξ_j^B is a 3x1 unit vector of the j^{th} satellite in the body frame, λ_{GNSS} is the wavelength of GNSS and $p_{m,n}$ is the 3x1 position vector of the $(m,n)^{th}$ antenna element in the body frame. Normally, the AOAs of the satellites are obtained in the navigation frame such as East-North-Up (ENU) and need to be rotated to body frame as

$$\xi_j^B = \mathbf{R}_{ENU}^B \xi_j^{ENU} \quad (3)$$

where, $\xi_j^{ENU} = \left[\cos\theta_j \sin\varphi_j \;\; \cos\theta_j \cos\varphi_j \;\; \sin\theta_j\right]$ and $\mathbf{R}_{ENU}^B$ is the rotation matrix from ENU to body frame using the roll, pitch and heading of the vehicle. The rotation matrix from ENU to body frame is given by equation 4 where, $\{r,p,a\}$ are the roll, pitch and heading (azimuth) of the vehicle.

2.3 RISS Mechanization

Herein, the vertical gyroscope was mounted in alignment with the vertical axis of the vehicle and two accelerometers were mounted in the transversal and forward directions. The gyroscope is used to measure the heading of the vehicle and the two accelerometers measured its roll and pitch. The vehicle attitude information along with odometer derived forward speed is then used to compute the velocity in ENU frame. Subsequently, 3D user positions are obtained by integrating the velocity solutions. The detailed mechanization process for RISS is available in [17].

$$\mathbf{R}_{ENU}^{B} = \begin{matrix} \cos(a)\cos(r) - \sin(r)\sin(p)\sin(a) & -\sin(a)\cos(p) & \cos(a)\sin(r) + \sin(r)\sin(p)\sin(a) \\ \sin(a)\cos(r) + \sin(r)\sin(p)\sin(a) & \cos(a)\cos(p) & \sin(a)\sin(r) - \cos(r)\sin(p)\cos(a) \\ -\sin(r)\cos(p) & \sin(p) & \cos(p)\cos(r) \end{matrix} \quad (4)$$

The mechanization equation to compute the vehicle attitude information are

$$p = -\sin^{-1}\left(\frac{f_y - a_{od}}{g}\right)\Delta t$$

$$r = -\sin^{-1}\left(\frac{f_x + v_{od}\omega_z}{g\cos p}\right)\Delta t \quad (5)$$

$$a = -\left[\omega_z - \omega^e \sin\emptyset - \frac{v_e \tan\phi}{R_N + h}\right]\Delta t$$

where $\{r, p, a\}$ are the roll, pitch and heading of the vehicle, f_x and f_y are the accelerometer measurements, a_{od} is the odometer measured acceleration, v_{od} is the odometer derived speed, ω_z is the vertical gyroscope measurement, ϕ is the latitude and h is the height.

The velocity in ENU frame are obtained using

$$v_e = v_{od}\sin(a)\cos(p)\,\Delta t$$

$$v_n = v_{od}\cos(a)\cos(p)\,\Delta t \quad (6)$$

$$v_u = v_{od}\sin(p)\,\Delta t$$

User positions are obtained using

$$\phi = \frac{v_n}{\mathrm{R}_m + h}\Delta t$$

$$\lambda = \frac{v_e}{(\mathrm{R}_n + h)\cos(\phi)}\Delta t \quad (7)$$

$$h = v_u \Delta t$$

2.4 Loosely Coupled Integration

In the loosely coupled integration approach, GNSS and RISS position solutions are combined using a Kalman filter. Both system and measurement model are nonlinear. As linearization is performed, only perturbations in the states are computed in the Kalman filter. The linearized system model is given by

$$\delta\boldsymbol{x}_{k+1} = \boldsymbol{\Phi}_{k,k+1}\delta\boldsymbol{x}_k + \mathbf{G}_k\mathbf{w}_k \quad (8)$$

where,

$\delta\boldsymbol{x}_k$ is the 9x1 error state vector at time epoch k given by $\delta\boldsymbol{x}_k = \{\delta\boldsymbol{\phi_k}\ \delta\lambda_k\ \delta h_k\ \delta v_k^E\ \delta v_k^N\ \delta v_k^U\ \delta A_k\ \delta S_k^{od}\ \delta\omega_k^z\}$

$\{\boldsymbol{\phi_k}\ \lambda_k\ h_k\}$ is the position vector in the geodetic coordinate frame

$\{v_k^E\ v_k^N\ v_k^U\}$ is the velocity vector in East-North-Up (ENU) coordinate frame

A_k is the azimuth angle

S_k^{od} is the scale factor of the odometer

ω_k^z is the vertical gyro drift

$\boldsymbol{\Phi}_{k,k+1}$ is the state transition matrix from epoch k to k+1,

$\mathbf{G}_k$ is the shaping matrix or noise coupling matrix and

$\mathbf{w}_k$ is the zero mean unity variance white noise.

The linearized system model is given by equation 9 where γ_{od} and $\gamma_{\omega\mathrm{z}}$ are the inverse of the autocorrelation time for odometer and gyroscope stochastic errors, σ_{od}^2 and $\sigma_{\omega\mathrm{z}}^2$ are the variance of the odometer and gyroscope noise. Details of deriving the state transition matrix are provided in [17, 18]. The linearized measurement model is given by

$$\delta\boldsymbol{z}_k = \mathbf{H}\delta\boldsymbol{x}_k + \boldsymbol{\epsilon_k} \quad (10)$$

where $\delta\boldsymbol{z}_k$ is the measurement vector given by

$$\delta\boldsymbol{z}_k = \begin{bmatrix} \phi_k^{GPS} - \phi_k^{RISS} \\ \lambda_k^{GPS} - \lambda_k^{RISS} \\ h_k^{GPS} - h_k^{RISS} \\ v_k^{E,GPS} - v_k^{E,RISS} \\ v_k^{N,GPS} - v_k^{N,RISS} \\ v_k^{U,GPS} - v_k^{U,RISS} \end{bmatrix} \quad (11)$$

$\mathbf{H}$ is the design matrix and $\boldsymbol{\epsilon_k}$ represents the measurement noise.

2.5 Interference Generation

The number of interference sources that an antenna array can mitigate depends on its number of antenna elements. Here, a four-element antenna array is considered that can mitigate up to three interference sources. Interference signals considered in this research are spoofing and wide band interference signals.

As it is prohibited to propagate interference signals in the outdoors, they are generated through software scripts and added to the Intermediate Frequency (IF) data samples collected beforehand. For generating spoofing signals, the GNSS signal simulator described in [19] was modified. Its architecture to generate different spoofing scenarios is shown in Figure 2. In this research, an overlapped spoofing scenario is considered. In such case, spoofing signals first align their correlation peaks with those of the authentic ones and subsequently shift the peaks. Using the software spoofing simulator, authentic signals are tracked to obtain the code phase and Doppler values for all visible satellites. For a few seconds, spoofing signals are then generated with the same code phase and Doppler values as those of authentic signals simulating an overlapped spoofing scenario. Later, precomputed delta code phase and Doppler values are added to the spoofing signals. In time-push spoofing scenario the same delta code phase and Doppler values are added to all the satellites to generate the spoofing signals. As the GNSS receiver used here is a multi-antenna one, the generated spoofing signals need to be modified to accommodate multi-antenna processing.

$$\begin{bmatrix} \delta\phi_k \\ \delta\lambda_k \\ \delta h_k \\ \delta v_k^E \\ \delta v_k^N \\ \delta v_k^U \\ \delta A_k \\ \delta S_k^{od} \\ \delta\omega_k^z \end{bmatrix} = \begin{bmatrix} 1 & 0 & 0 & 0 & \frac{\Delta t}{R_m + h_{k-1}} & 0 & 0 & 0 & 0 \\ 0 & 1 & 0 & \frac{\Delta t}{(R_n + h_{k-1})\cos(\phi_{k-1})} & 0 & 0 & 0 & 0 & 0 \\ 0 & 0 & 1 & 0 & 0 & \Delta t & 0 & 0 & 0 \\ 0 & 0 & 0 & 0 & 0 & 0 & v_{od}\cos(a_{k-1})\cos(p_{k-1})\Delta t & v_{od}\sin(a_{k-1})\cos(p_{k-1})\Delta t & 0 \\ 0 & 0 & 0 & 0 & 0 & 0 & v_{od}\sin(a_{k-1})\cos(p_{k-1})\Delta t & v_{od}\cos(a_{k-1})\cos(p_{k-1})\Delta t & 0 \\ 0 & 0 & 0 & 0 & 0 & 0 & 0 & v_{od}\sin(p_{k-1})\Delta t & 0 \\ 0 & 0 & 0 & 0 & 0 & 0 & 1 & 0 & 0 \\ 0 & 0 & 0 & 0 & 0 & 0 & 0 & 1-\gamma_{od}\Delta t & -\Delta t \\ 0 & 0 & 0 & 0 & 0 & 0 & 0 & 0 & 1-\gamma_{\omega z}\Delta t \end{bmatrix} \begin{bmatrix} \delta\phi_{k-1} \\ \delta\lambda_{k-1} \\ \delta h_{k-1} \\ \delta v_{k-1}^E \\ \delta v_{k-1}^N \\ \delta v_{k-1}^U \\ \delta A_{k-1} \\ \delta S_{k-1}^{od} \\ \delta\omega_{k-1}^z \end{bmatrix} + \begin{bmatrix} 0 \\ 0 \\ 0 \\ 0 \\ 0 \\ 0 \\ 0 \\ \sqrt{2\gamma_{od}\sigma_{od}^2\Delta t} \\ \sqrt{2\gamma_{\omega z}\sigma_{\omega z}^2\Delta t} \end{bmatrix} \quad (9)$$

Attitude of the antenna array and array calibration were considered while simulating the multi-antenna signals.

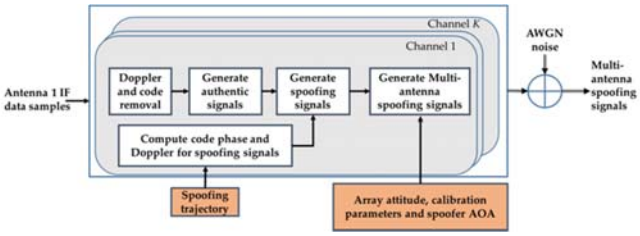

Figure 2: Multi-antenna spoofing signal generation

During the initial 40 seconds of the spoofing generation, it is assumed that spoofing signals perfectly overlaps with authentic signals as shown in Figure 3. After 40 s, spoofing signal code phase slowly moves away from the authentic signals. Once authentic and spoofing signals are separated by two chips, spoofer basically follows the predefined spoofing trajectory to mislead the user trajectory. Here, it is assumed that spoofing signals power is 3 dB higher than those of authentic signals. The authentic and spoofing trajectories are shown in Figure 4. An arbitrary spoofing trajectory was simulated by adding linear increments to both latitude and longitude.

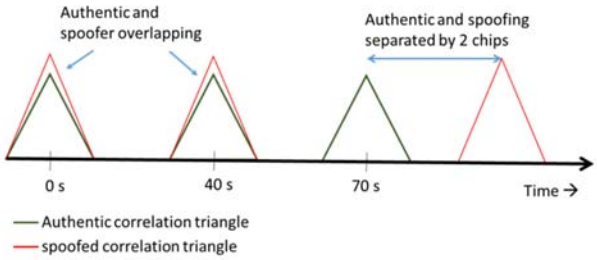

Figure 3: Overlapped spoofing simulation description

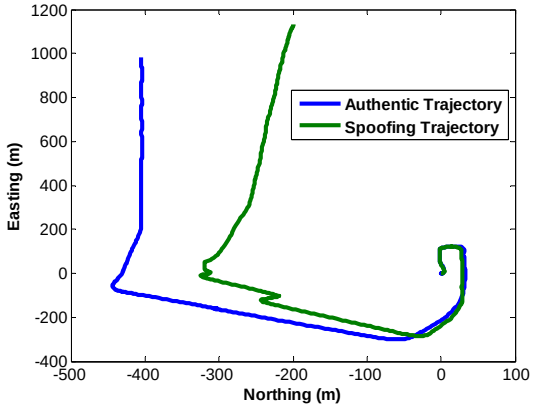

Figure 4: Authentic and spoofing trajectories

2.6 Performance of antenna array for mitigation of overlapping spoofing attacks

In an overlapped spoofing attack, the spoofer first overlaps its correlation peaks with those of authentic ones and then tries to take control of the receiver tracking correlators. When the authentic and spoofing signals overlap, there is a high correlation between authentic and spoofing signals that affects the performance of the antenna array spoofing mitigation. Hence, it is of interest to characterize the performance of spoofing mitigation as a function of relative authentic spoofing delay. Performance of the MPDR beamformer for overlapped spoofing scenario is evaluated. Since the covariance matrix is computed before the correlation process in the present approach, MPDR can essentially mitigate spoofing signals without the need for spatial smoothing. Figure 5 shows the performance of the MPDR beamformer for different values of relative authentic-spoofing delays. It can be observed that as spoofing correlation peak moves away from the authentic ones, a better attenuation of spoofing signals is obtained. MPDR beamformer performance degrades in the presence of correlated signals. When the authentic and spoofing signals perfectly overlap, there is a high correlation between them. When overlapping between authentic and spoofing decreases, there is more decorrelation between authentic and spoofing signals which improves the performance of the MPDR beamformer.

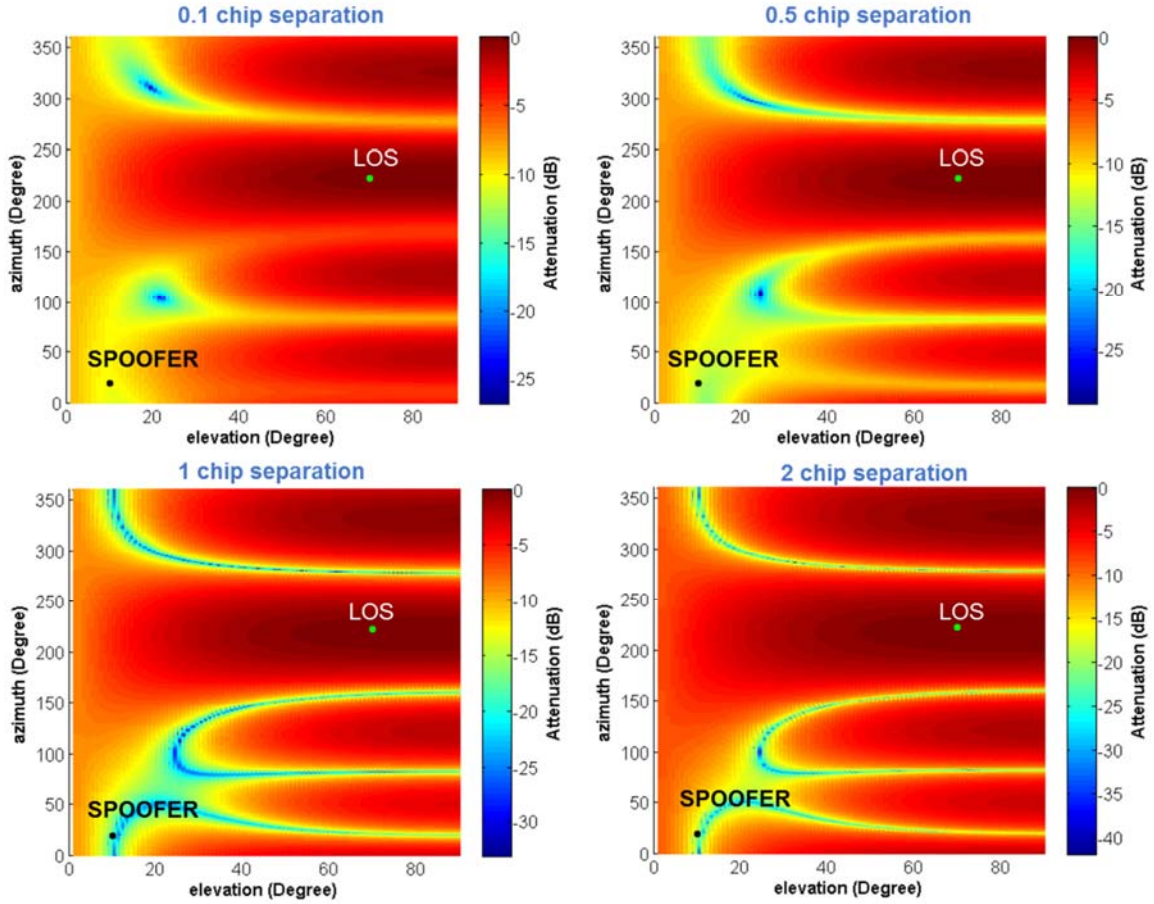

Figure 5: Spoofing mitigation performance with MPDR beamformer for different code phase overlapping scenarios

Figure 5 also shows that when the correlation peak separation is 0.1 chips, spoofing signals can be attenuated by up to 10 dB. When the correlation peaks are separated by 0.5 chips, an attenuation of nearly 20 dB occurs. For more than 1 chip separation, attenuation of 25 dB to 30 dB occurs.

3 DATA COLLECTION AND PROCESSING

Data was collected by mounting the antenna array on the top of a vehicle as shown in Figure 6a. The rectangular antenna array was constructed with four elements using Novatel 501 antennas. On the same platform, two different types of IMUs, namely tactical and automotive grades, were mounted. The tactical grade IMU integrated with a GNSS receiver was used to provide a reference trajectory. The specifications of the automotive grade IMU used in the antenna array coupling are provided in Table 1. A multi-antenna RF front-end was used to collect data from all the antennas simultaneously. The AOA of visible satellites along with that of the spoofer (S) and wideband interference (INT) are shown in Figure 6b. The simulated wideband interference occupies the entire GNSS bandwidth with a jammer-to-noise ratio of 20 dB.

Table 1: IMU error characteristics

IMU Type	Sensors	value	White noise
Automotive	Accel. bias	16 mg	60 µg/√Hz
	Gyroscope drift	12 °/hr	0.02 °/s/√Hz

The data was processed in different cases as described below. In all cases, performance of single antenna, antenna array, GPS-RISS and Antenna array GPS-RISS are analysed:

Case1: Only authentic signals are considered.
Case2: Authentic and spoofing signals are considered.
Case3: Authentic, spoofing and wide band interference are considered.
Case4: GNSS outages are considered

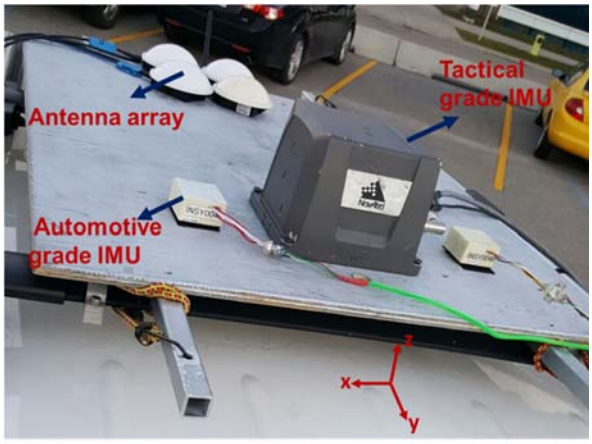

(a)

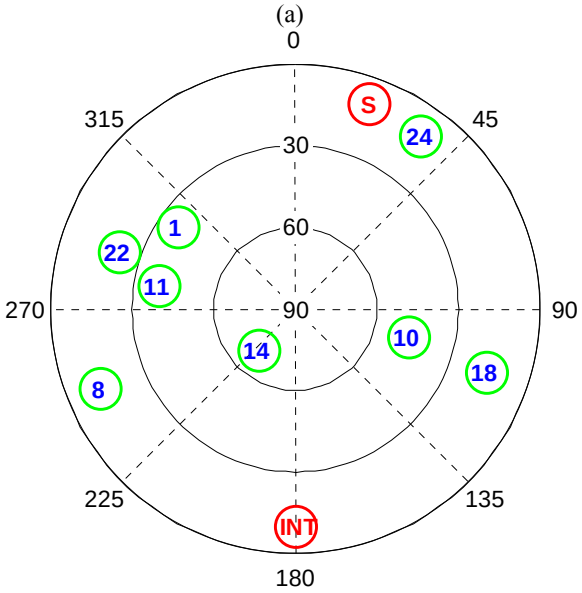

(b)

Figure 6: (a) Data collection setup and (b) sky plot showing visible satellites, spoofer and wideband interference

4 RESULTS AND DISCUSSIONS

This section provides results of multi-antenna GPS and INS-odometer integration in different scenarios as a function of navigation solution performance in the presence of spoofing and interference signals.

4.1 Case1: Only authentic signals

The performance of single antenna and antenna array integration with RISS using a clean data set is analysed. The data was collected in open sky conditions with a clear view of satellites. Figure 7a shows position errors as a function of time for the single antenna case. GPS and GPS-RISS solutions are almost the same, showing the limited availability and accuracy improvement that can be achieved by integrating GPS with an automotive grade IMU. Figure 7b shows the performance of the GPS antenna array and GPS-RISS integration. Table 2 provides the statistics for the above cases. As shown, the GPS and GPS-RISS performance metrics with a clean data set are almost the same. The obvious reason is that in open sky conditions with high quality GPS measurements, the navigation filter puts high weight on the GPS measurements. Hence, GPS and GPS-RISS solutions are dominated by GPS. The performance of single antenna and antenna array GPS receivers under open sky conditions is also the same. This is due to the fact that in this scenario with low multipath and no RF interference, the advantage of antenna array processing over that of a single antenna is limited to improvement in signal-to-noise ratio. The actual advantage of antenna array processing over single antenna receiver is for interference and spoofing mitigation as will be shown in the next scenarios.

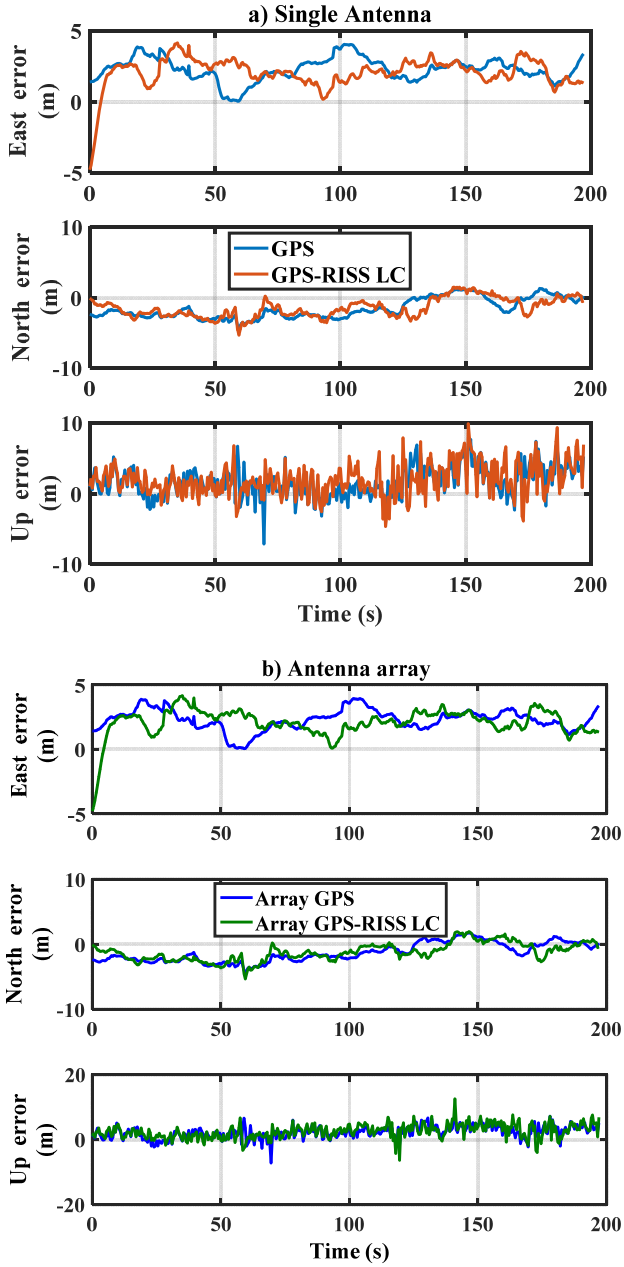

Figure 7: ENU position errors with (a) Single antenna GPS and GPS-RISS LC (b) Antenna array GPS and GPS-RISS LC

4.2 Case2: Authentic and spoofing signals

In this case, the spoofing signals were generated and added to the clean data set as described in the previous section. In this case, it is of interest to compare the performance of GPS only, GPS-RISS and antenna array GPS-RISS under a spoofing attack. In the case of antenna array processing, a spoofing detection method based on Eigen analysis of the spatial pre-despreading covariance matrix was developed. The steering vector of the spoofing signals were estimated based on the Eigenvector corresponding to the largest Eigen value of the pre-despreading covariance matrix. A MPDR beamformer using heading information from RISS and direction of arrival of authentic signals were then employed to place a null in the direction of spoofing signals and steer a beam toward each PRN. Figure 8a shows the performance of single antenna GPS and GPS-RISS under the spoofing attack. Navigation solutions are spoofed for both GPS and GPS-RISS solutions. Figure 8b shows horizontal trajectories using the antenna array for both GPS and GPS-RISS scenarios. Antenna array processing successfully detects and mitigates the spoofing signals and the resulting trajectory agrees with the authentic one. Table 3 provides the navigation solutions error statistics for these cases.

4.3 Case3: Authentic in the presence of spoofing and wideband interference

In this case, the receiver was attacked by both spoofing and a wideband jammer. The direction of arrival of the spoofing and jamming signals are provided in Figure 6. The wideband interference degraded the C/N_0 values; however, it did not cause loss of lock on any tracking channels. Hence the number of PRNs used in the navigation solutions was the same as in previous cases. Figure 9a shows the performance of single antenna GPS and GPS-RISS under jamming and spoofing attacks in which solutions are spoofed for both GPS and GPS-RISS. Figure 9b shows the trajectories using antenna array for both GPS and GPS-RISS scenarios. Antenna array processing successfully detects and mitigates the jamming and spoofing signals and the resulting trajectory matches the authentic one. Table 4 provides the navigation solutions error statistics for these cases.

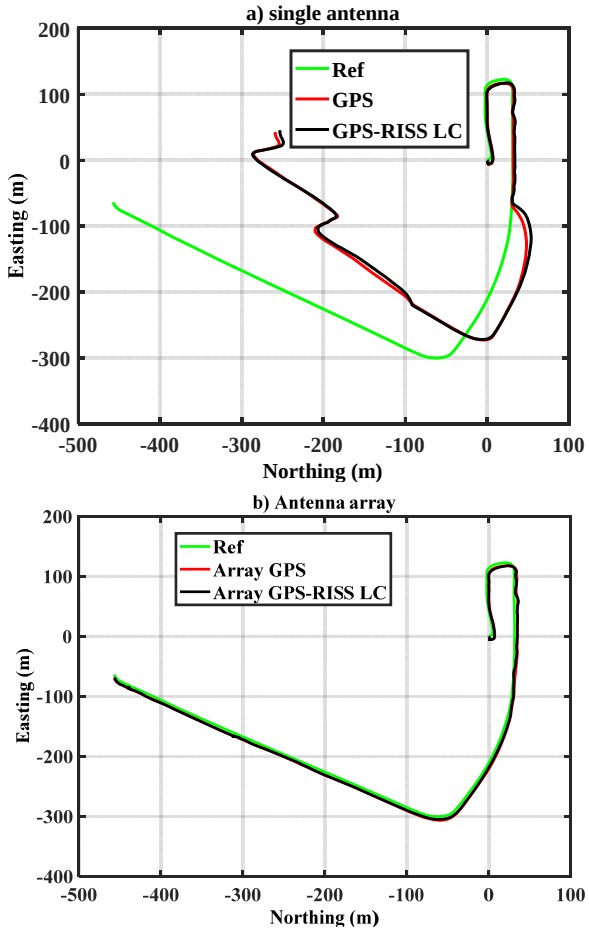

Figure 8: Trajectories in the presence of spoofing signals with (a) Single antenna GPS and GPS-RISS LC (b) Antenna array GPS and GPS-RISS LC solutions

Table 2. ENU position errors statistics with authentic signals

Position errors	North error (m)		East error (m)		Up error (m)	
	Mean	Standard deviation	Mean	Standard deviation	Mean	Standard deviation
GPS	2.3	0.8	-1.5	1.4	1.6	2.1
GPS-RISS LC	2.1	0.7	-1.4	1.3	1.9	2.3
Array GPS	2.2	0.8	-1.2	1.4	1.3	1.9
Array GPS-RISS LC	2.2	0.7	-1.2	1.3	1.2	2.1

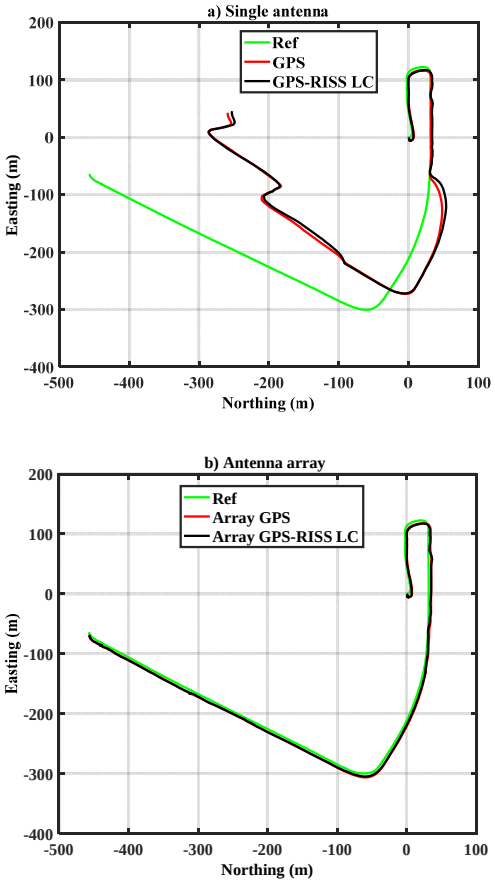

Figure 9: Trajectory in the presence of spoofing and wideband interference with (a) Single antenna GPS, and GPS-RISS LC (b) Antenna array and GPS-RISS LC solutions

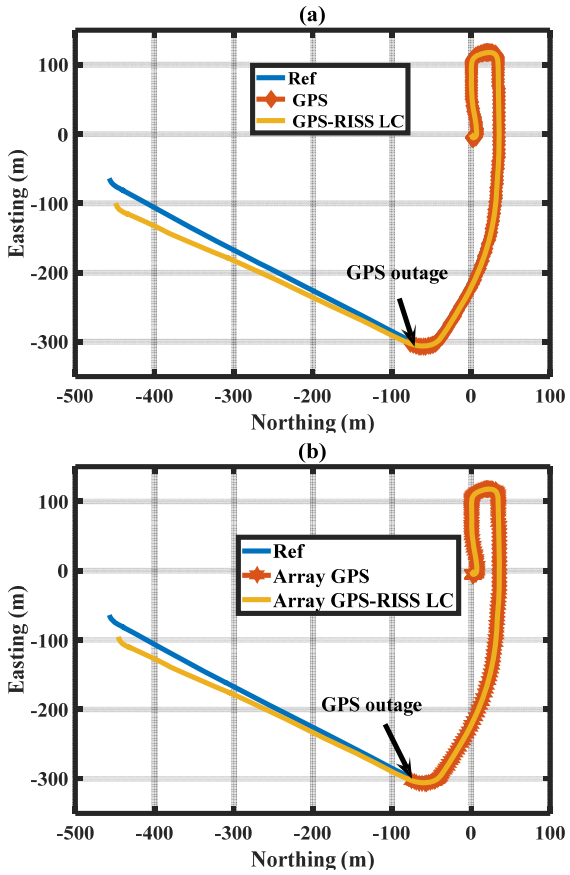

Figure 10: Trajectory during outage in the presence of spoofing and wideband interference with (a) Single antenna GPS, and LC solutions (b) Antenna array and LC solutions

4.4 Case4: Outage scenario

In this case, the performance of GPS-INS integration under GPS outage was investigated. The GPS signals after 200 s from the beginning was attenuated to the point that single and antenna array GPS receivers lost lock in all tracking channels. Figure 10 shows the trajectory of the receiver before and after the outage. The solutions of the single antenna and GPS antenna array integrated with RISS-odometer before the outage are the same. Single antenna and antenna array receivers could not provide navigation solutions after GPS outage. However, the GPS receivers integrated with RISS did provided solutions in this case. The solutions however deviate from the actual trajectory. This error is a function of the initial navigation solutions error at the outage epoch and characteristics of the IMU. The antenna array solutions integrated with RISS after the outage has less error compared to the single antenna and RISS integration case which is due to the better navigation solution estimation before outage.

Table 5 provides navigation solutions statistics for single antenna and antenna array GPS integrated with RISS.

5 SUMMARY AND CONCLUSIONS

The performance of single and multi-antenna GPS receivers integrated with INS and odometer data were investigated under spoofing, jamming and GPS outage cases for vehicular navigation. Results showed that under open sky conditions, the performance of the antenna array and antenna array coupled with RISS are very similar to that of a single antenna GPS receiver. In the presence of spoofing signals, the signal antenna and GPS/RISS receiver were spoofed whereas the antenna array-RISS-integration detected and mitigated the spoofing signals. In the presence of jamming signals, the performance of signal antenna receiver was significantly degraded due to the jamming effect whereas the antenna array-RISS integration provided continuous high quality measurements. In the presence of GPS outages, the performance of GPS-INS integration degraded due to inherent IMU drifts. The performance of antenna array GPS-INS coupling was slightly better than that of single antenna GPS-INS integration.

Table 3. ENU position errors statistics with authentic and spoofing signals

Position errors	North error (m)		East error (m)		Up error (m)	
	Mean	Standard deviation	Mean	Standard deviation	Mean	Standard deviation
GPS	-50.9	54.2	-66.4	61.4	2.9	10.8
GPS-RISS LC	-51.8	54.2	-67.3	61.5	-3.2	12.3
Array GPS	2.7	0.8	-1.3	1.4	2.4	1.9
Array GPS-RISS LC	2.2	0.7	-1.2	1.3	1.2	2.2

Table 4. ENU position errors statistics with authentic, spoofing and wideband interference signals

Position errors	North error (m)		East error (m)		Up error (m)	
	Mean	Standard deviation	Mean	Standard deviation	Mean	Standard deviation
GPS	-50.9	55.2	-67.2	61.7	3.4	15.2
GPS-RISS LC	-51.8	54.2	-68.3	61.5	2.9	12.3
Array GPS	2.7	0.9	-1.3	1.4	2.5	2.1
Array GPS-RISS LC	2.2	0.7	-1.2	1.3	1.8	2.5

Table 5. ENU position errors statistics with outages

Position errors	North error (m)		East error (m)		Up error (m)	
	Mean	Standard deviation	Mean	Standard deviation	Mean	Standard deviation
GPS-RISS LC	19.4	16.3	-1.2	1.9	-9.6	14.3
Array GPS-RISS LC	14.2	10.8	-3.3	2.5	-8.8	14.1

REFERENCES

1. Park, M.; Gao, Y. Error and performance analysis of MEMS-based inertial sensors with a low-cost GPS receiver. *Sensors* 2008, *9*, 2240–2261.
2. Godha, S.; Cannon, M.E. GPS/MEMS INS integrated system for navigation in urban areas. *GPS Solut* 2007, *11*, 193–203.
3. Bijker, J.; Steyn, W. Kalman filter configurations for a low-cost loosely integrated inertial navigation system on an airship. *Control Eng. Pract* 2008, *16*, 1509–1518.
4. Angrisano, A.; Petovello, M.; Pugliano, G. Benefits of Combined GPS/GLONASS with Low-Cost MEMS IMUs for Vehicular Urban Navigation. *Sensors* 2012, *12*, 5134-5158.
5. Georgy J, Noureldin A, Korenberg M, Bayoumi M. Low Cost Three Dimensional Navigation Solution for RISS/GPS Integration Using Mixture Particle Filter. IEEE Trans. Vehicul. Technol. 2010;59:599–615.
6. Fernández-Prades, C.; Arribas, J.; Closas, P. Robust GNSS Receivers by Array Signal Processing: Theory and Implementation. *Proceedings of the IEEE*, 2016, *vol.PP*, no.99, pp1-14.
7. Gupta, I.J.; Weiss, I.M.; Morrison, A.W. Desired Features of Adaptive Antenna Arrays for GNSS Receivers. *Proceedings of the IEEE* , 2016, *vol.PP*, no.99, pp.1-12.
8. Cuntz, M.; Konovaltsev, A.; Meurer, M. Concepts, Development, and Validation of Multiantenna GNSS Receivers for Resilient Navigation. *Proceedings of the IEEE* ,2016, *vol.PP*, no.99, pp.1-14.
9. Amin, M.G.; Wang, X.; Zhang, Y.D. ; Ahmad, F.; Aboutanios E. Sparse Arrays and Sampling for Interference Mitigation and DOA Estimation in GNSS. *Proceedings of the IEEE* ,2016, *vol.PP*, no.99, pp.1-16.
10. Broumandan, A.; Jafarnia-Jahromi, A.; Daneshmand, S.; Lachapelle, G. Overview of Spatial Processing Approaches for GNSS Structural Interference Detection and Mitigation. *Proceedings of the IEEE* , 2016 *vol.104*, no.99, pp.1246-1257.

11. Psiaki, M.L.; Humphreys, T.E. GNSS Spoofing and Detection. *Proceedings of the IEEE* ,2016, *vol. 104, no. 6, pp. 1258-1270, June* 2016
12. Jafarnia, A.; Broumandan, A.; Nielsen,J.; Lachapelle, G. GPS spoofer countermeasure effectiveness based on using signal strength, noise power and C/N0 observables. *Int. J. Satellite Commun. Netw., vol. 30, no. 4, pp. 181–191, Jul.* 2012
13. Akos, D. M. Who's afraid of the spoofer? GPS/GNSS spoofing detection via automatic gain control (AGC) *Journal of Navigation, vol. 59, no. 4, pp. 281–290,* 2012*, Winter, Institute of Navigation*.
14. Jafarnia, A.; Broumandan,A.; Nielsen,J.; Lachapelle,G. Pre-despreading authenticity verification for GPS L1 C/A signals. *J. Inst. Navig., vol. 61, no. 1, pp. 1–11,* 2014
15. Nielsen, J.; Dehghanian,V.; Lachapelle,G. Effectiveness of GNSS spoofing countermeasure based on receiver CNR measurements. *Int. J. Navig. Observations, vol. 2012, p. 9,* 2012*, Art. no. 501679*
16. Swaszek, P. F.; Pratz, S. A.; Arocho, B. N.; Seals, K. C.; Hartnett, R. J. GNSS spoof detection using shipboard IMU measurements*. in Proc. ION GNSS + 14, Tampa, FL, USA, Sep. 8–12,* 2014*, pp. 745–758*
17. Khanafseh, S.; Roshan, N.; Langel, S.; Fang-Cheng Chan,C.; Joerger, M.; Pervan, B; GPS Spoofing Detection using RAIM with INS Coupling. *Position, Location and Navigation Symposium - PLANS* 2014, *Monterey, CA, USA, pp. 1232–1239*
18. Grejner-Brzezinska, A.D.; Toth, C. K.; Moore,T.; Raquet, J. F.; Miller, M. M.; Kealy, A. Multisensor Navigation Systems: A Remedy for GNSS Vulnerabilities?. *Proceedings of the IEEE* ,2016, *vol. 104, no. 6, pp. 1339-1353, June* 2016.
19. Daneshmand, S.; Jafarnia, A.; Broumandan, A.; Lachapelle, G. A low-complexity GPS anti-spoofing method using a multi-antenna array. *in Proc. ION GNSS* 2012*, Nashville, TN, USA, Sep. 17–21, 2012, p. 11.*
20. Cuntz, M.; Konovaltsev, A.; Meurer, M. Concepts, Development, and Validation of Multiantenna GNSS Receivers for Resilient Navigation. *Proceedings of the IEEE* ,2016, *vol.PP*, no.99, pp.1-14.
21. A. Noureldin et al., Fundamentals of Inertial Navigation, Satellite-based Positioning and their Integration, DOI: 10.1007/978-3-642-30466-8_4, _ Springer-Verlag Berlin Heidelberg 2013
22. Karamat, T.B.; Georgy, J.; Iqbal, U.; Noureldin, A. A Tightly-Coupled Reduced Multi-Sensor System for Urban Navigation. In Proceedings of the 22nd International Technical Meeting of the Satellite Division of the Institute of Navigation-ION GNSS 2009, Savannah, GA, USA, 22–25 September 2009; pp. 582–592
23. Vagle, N., A. Broumandan, A. Jafarnia-Jahromi and G. Lachapelle (2016) Performance Analysis of GNSS Multipath Mitigation using Antenna Arrays. The Journal of Global Positioning Systems, 15 pages;DOI 10.1186/s41445-016-0004-6
24. Novatel GPSAntennaTM model 501, avialabel at http://www.novatel.com/assets/Documents/Manuals/om-20000001.pdf (Accessed 10 January 2017).